AIMS Mathematics, 10(1): 1142–1161.
DOI: 10.3934/math.2025054
Received: 20 November 2024
Revised: 03 January 2025
Accepted: 08 January 2025
Published: 20 January 2025

https://www.aimspress.com/journal/Math

Research article

Adaptive smooth sampled-data control for synchronization of T–S fuzzy reaction-diffusion neural networks with actuator saturation

Yuchen Niu[1], **Kaibo Shi**[1,2,*], **Xiao Cai**[3] **and Shiping Wen**[4]

[1] College of Electrical Engineering, Sichuan University, Chengdu, Sichuan 610065, China
[2] School of Electronic Information and Electrical Engineering, Chengdu University, Chengdu, Sichuan 610106, China
[3] Cyberspace Institute of Advanced Technology, Guangzhou University, Guangzhou 510006, China
[4] Faculty of Engineering and Information Technology, Australian AI Institute, University of Technology Sydney, Ultimo, NSW 2007, Australia

* **Correspondence:** Email: shikaibo@cdu.edu.cn.

Abstract: This paper addresses the synchronization issue in T–S fuzzy reaction–diffusion neural networks (TFRNNs) with time-varying delays and actuator saturation. First, an adaptive smooth sampled-data (ASSD) controller is proposed to optimize communication resources. In the ASSD controller, the dynamic forgetting factor is employed to process historical data smoothly, thereby preventing data distortion due to unexpected events. Second, the Lyapunov–Krasovskii functional (LKF), which captures more information about the system, is introduced, and it can provide greater flexibility than the fixed-matrix LKF. Meanwhile, by employing the semi-looped-functional method, the constraint for negative determination of the sum of its derivatives is removed, which enhances the feasibility of expanding the solution. Consequently, a novel criterion and the corresponding algorithm are established to obtain the larger maximum allowable sampling interval (MASI). Finally, simulations demonstrate the effectiveness and superiority of the proposed theoretical results.

Keywords: T–S fuzzy reaction–diffusion neural networks; sampled-data control; synchronization; Lyapunov–Krasovskii functional
Mathematics Subject Classification: 35B35, 93C42, 93C43, 96D21

1. Introduction

In recent years, Takagi–Sugeno fuzzy neural networks (TSFNNs), which are hybrid systems combining fuzzy logic and neural networks (NNs), have garnered considerable research interest because of their applications in nonlinear systems [1–4]. TSFNNs define input and output variables

using fuzzy sets and fuzzy logic-based rules to establish their relationship, effectively capturing dynamic information in physical systems [5–8]. In many domains, ranging from intelligent transportation systems, financial risk analysis, medical diagnostics, and intelligent robotics, TSFNNs have been widely applied. Synchronization, a critical dynamic behavior in TSFNNs, continues to be a significant research focus. Synchronization can occur naturally or be achieved by design and has critical applications in communication systems, image encryption, and power systems [9–12]. In [13], TFSNN synchronization was used for image encryption, effectively concealing and restoring the original image. Thus, the study of synchronization holds significant importance.

Various factors influence the states of TSFNNs. Accurately describing these states requires considering the effects of time delays and reaction–diffusion phenomena [14–17]. Appropriately timed delays can reduce oscillatory tendencies in a system and promote faster convergence. However, time delays can also result in the degradation of the system performance or even destabilization [18–20]. Therefore, it is crucial to account for the effects of delays. The study in [19] focused on observer-based dissipativity control in TSFNNs with distributed delays. Li et al. [20] addressed the event-triggered stabilization of a novel T–S fuzzy complex-valued memristive NN with mixed time-varying delays. Additionally, TSFNNs inherently exhibit the reaction–diffusion phenomenon due to environmental influences. This suggests that changes in the system's state depend not only on time but also on the spatial context. TFRNNs can better characterize the evolution of neurons during time and spatial changes. TFRNNs are more realistic than traditional TSFNNs. The study in [21] addressed the outlier-resistant nonfragile control problem in TFRDNNs. Liu et al. [22] explored the H_∞ state estimation problem in TFRNNs, considering gain uncertainties and semi-Markov jump parameters.

In modern control systems, digital computers are usually used for data signal acquisition and measurement analysis, with the help of discrete-time SD controllers for controlling continuous-time objects to realize the control function of the system [23–27]. This control method is called SD control and is widely used in solving synchronization problems. You et al. [25] explored the issue of exponential synchronization in inertial NN examined within the context of aperiodic sampling and state quantization. The study in [26] addressed exponential synchronization in TFRNNs with additive time-varying delays using both time SD control and time–space SD control. The study in reference [27] employed a memory-based SD controller to investigate the synchronization of NNs in the presence of parameter uncertainties. Most SD controls are built using data either at the current moment or from previous moments. In reality, measured data can exhibit random fluctuations or anomalies. These errors can manifest in various forms, including loss or anomalies in data from node task conflicts and sampling jitter caused by hardware aging. Consequently, these issues may affect sampling measurement results, potentially causing redundant data transmission. Moreover, memory-based SD controllers inherently consume storage space. A very small sampling interval may deplete storage space, rendering the system inoperable. In summary, we propose using an ASSD controller to mitigate these challenges. This approach also provides further motivation for the research presented in this paper.

Inspired by the discussions above, we aim to explore the synchronization of TFRNNs with time-varying delays through the design of ASSD control. Table 1 lists fundamental mathematical symbols, and the primary contributions of this study are summarized as follows:

(1) This study offers a comprehensive view of the synchronization of TFRNNs, considering factors such as ASSD, reaction–diffusion and actuator saturation, thereby enhancing the applicability of the

results.

(2) The improved ASSD controller uses the dynamic forgetting factor to allocate current and historical measurements, effectively countering data distortion and improving the system's control performance.

(3) The LKFs with membership function and time-varying delays correlation capture system information comprehensively. Furthermore, the compensation LKF $V_3(t)$ and the fuzzy zero equation are employed to address the integral term with the membership function's derivatives, increasing the feasible range of matrix variables.

(4) Unlike the traditional LKF method, the semi-looped-functional method does not require the sum of its derivatives to be negative definite. This results in the derivation of a synchronization criterion with more relaxed constraints.

Table 1. Notations and descriptions.

Notation	Description
$\mathbf{sym}\{X\}$	$X + X^T$
$\mathbf{col}\{\cdots\}$	a column vector
$\mathbf{diag}\{\cdots\}$	a block-diagonal matrix
R^n	the n-dimensional Euclidean space
$R^{n\times m}$	the set of all $n \times m$ real matrices
I_n	an $n \times n$ identity matrix
$0_{n\times m}$	an $n \times m$ zero matrix
$\|\varsigma(t,x)\|$	$\|\varsigma(t,x)\| = (\int_\Gamma \varsigma^T(t,x)\varsigma(t,x)dx)^{(1/2)}$
$C([-\bar{\sigma},0]\times\Gamma, R^n)$	all continuous functions mapping from $[-\bar{\sigma},0]\times\Gamma$ to R^n

2. Preliminaries and problem formulation

The TFRNNs described by IF–THEN rules are considered as follows:

Plant rule i: IF $\mathscr{C}_1(t)$ is $\mathfrak{V}_1^i$, $\mathscr{C}_2(t)$ is $\mathfrak{V}_2^i$,..., and $\mathscr{C}_l(t)$ is $\mathfrak{V}_l^i$, then

$$\frac{\partial\varsigma(t,x)}{\partial t} = \sum_{l=1}^{\omega}\frac{\partial}{\partial x_l}(A_l\frac{\partial\varsigma(t,x)}{\partial x_l}) - B_i\varsigma(t,x) + C_i f(\varsigma(t,x)) + D_i f(\varsigma(t-\sigma(t),x)) + \mathfrak{T}(t), \tag{2.1}$$

where for each $i \in \mathfrak{F} \triangleq \{1,2,...,p\}$, $\mathscr{C}_\hbar$ and $M_\hbar^i$ ($\hbar = 1,...,p$) denote the $\hbar$th premise variable and its corresponding fuzzy set. $x = \mathbf{col}\{x_1, x_2, \ldots, x_\omega\}$ is the spatial variable within $\Gamma = [\underline{\alpha}_1, \overline{\alpha}_1] \times \ldots \times [\underline{\alpha}_\omega, \overline{\alpha}_\omega]$, and $\partial\Gamma$ denotes its boundary. The state vector $\varsigma(t,x) = \mathbf{col}\{\varsigma_1(t,x), \varsigma_2(t,x), \ldots, \varsigma_n(t,x)\}$ represents the system state. A_l represents the transmission diffusion coefficient; B_i indicates the neuron charging time constant; C_i and D_i represent the connection weight matrix, $\mathfrak{T}(t)$ is the external input, and $\sigma(t)$ denotes the time-varying delays that satisfy

$$0 \le \sigma(t) \le \bar{\sigma},\ \dot{\sigma}(t) \le \eth. \tag{2.2}$$

Utilizing the weighted average fuzzy blending approach, the TFRNNs are described as follows:

$$\frac{\partial \varsigma(t,x)}{\partial t} = \sum_{i=1}^{\iota} \mathfrak{h}_i(\mathscr{C}(t))\Big\{ \sum_{l=1}^{m} \frac{\partial}{\partial x_l}(A_l \frac{\partial \varsigma(t,x)}{\partial x_l}) - B_i\varsigma(t,x) + C_i f(\varsigma(t,x)) + \mathfrak{T}(t) + D_i f(\varsigma(t-\sigma(t),x))\Big\}, \quad (2.3)$$

where $\mathscr{C}(t) = \mathbf{col}\{\mathscr{C}_1(t), \mathscr{C}_2(t), ..., \mathscr{C}_l(t)\}$ and $\mathfrak{h}_i(\mathscr{C}(t))$ is the normalized membership function, and it satisfies

$$\begin{aligned} \mathfrak{h}_i(\mathscr{C}(t)) &= \frac{\mathfrak{V}^i(\mathscr{C}(t))}{\sum_{s=1}^{l} \mathfrak{V}^s(\mathscr{C}(t))} \geq 0, \ \sum\nolimits_{i=1}^{l} \mathfrak{h}_i(\mathscr{C}(t)) = 1, \\ \mathfrak{V}^i(\mathscr{C}(t)) &= \prod\nolimits_{j=1}^{l} \mathfrak{V}_j^i(\mathscr{C}_j(t)), \ \sum\nolimits_{i=1}^{l} \dot{\mathfrak{h}}_i(\mathscr{C}(t)) = 0, \end{aligned} \quad (2.4)$$

and the term $\mathfrak{V}_j^i(\mathscr{C}_j(t))$ represents the membership grade of $\mathscr{C}_j(t)$ in $\mathfrak{V}_j^i$.

Considering system (2.3) as the master system, the corresponding slave system is defined as follows:

$$\begin{aligned} \frac{\partial \bar{\varsigma}(t,x)}{\partial t} = \sum_{i=1}^{\iota} \mathfrak{h}_i(\mathscr{C}(t))\Big\{ \sum_{l=1}^{m} \frac{\partial}{\partial x_l}(A_l \frac{\partial \bar{\varsigma}(t,x)}{\partial x_l}) - B_i\bar{\varsigma}(t,x) + C_i f(\bar{\varsigma}(t,x)) + \mathfrak{T}(t) \\ + D_i f(\bar{\varsigma}(t-\sigma(t),x)) + u(t,x)\Big\}. \end{aligned} \quad (2.5)$$

The initial values and boundary conditions associated with systems (2.3) and (2.5) are specified as follows:

$$\begin{aligned} &\varsigma(t,x) = \bar{\varsigma}(t,x) = 0, \ (t,x) \in [t_0 - \bar{\sigma}, +\infty) \times \partial\Gamma, \\ &\varsigma(s+t_0,x) = \mathfrak{g}(s,x) \in C([-\bar{\sigma},0] \times \Gamma, R^n), \\ &\bar{\varsigma}(s+t_0,x) = \bar{\mathfrak{g}}(s,x) \in C([-\bar{\sigma},0] \times \Gamma, R^n). \end{aligned}$$

Define the error vector as $\psi(t,x) = \varsigma(t,x) - \bar{\varsigma}(t,x)$. Combining (2.3) and (2.5), the resulting error system is as follows:

$$\begin{aligned} \frac{\partial \psi(t,x)}{\partial t} = \sum_{i=1}^{\iota} \mathfrak{h}_i(\mathscr{C}(t))\Big\{ \sum_{l=1}^{m} \frac{\partial}{\partial x_l}(A_l \frac{\partial \psi(t,x)}{\partial x_l}) - B_i\psi(t,x) \\ + C_i g(t,x) + D_i g(t-\sigma(t),x) + u(t,x)\Big\}, \end{aligned} \quad (2.6)$$

where $g(t,x) = f(\varsigma(t,x)) - f(\bar{\varsigma}(t,x))$ satisfies

$$[g(t,x) - \Omega_1\psi(t,x)]^T[g(t,x) - \Omega_2\psi(t,x)] \leq 0, \quad (2.7)$$

and Ω_1, Ω_2 are constant matrices and $\Omega_2 \geq \Omega_1$.

Control rule j: IF $\mathscr{C}_1(t)$ is $\mathfrak{V}_1^j$, $\mathscr{C}_2(t)$ is $\mathfrak{V}_2^j$,..., and $\mathscr{C}_q(t)$ is $\mathfrak{V}_q^j$, then

$$u(t,x) = \mathcal{K}_j\psi(t,x), \quad (2.8)$$

where $\mathcal{K}_j$ are fuzzy the controller gains. By adopting a similar approach to that used for system (2.3), we obtain

$$u(t,x) = \sum_{j=1}^{\iota} \mathfrak{h}_j(\mathscr{C}(t))\mathcal{K}_j\psi(t,x). \quad (2.9)$$

Furthermore, considering the effects of SD, the states $\psi(t,x)$ can be measured at discrete sampling points t_k. Moreover, these samplings adhere to the assumption: $0 \leq d_k \triangleq t_{k+1} - t_k \leq d_M, (k = 1, 2, \ldots, \infty)$. Subsequently, an ASSD controller is employed to conserve communication resources and improve anti-interference capabilities. The weighted measurement is expressed as:

$$\begin{cases} \tilde{\psi}(t_{k+1},x) = \alpha(t_{k+1})\psi(t_{k+1},x) + (1-\alpha(t_{k+1}))\tilde{\psi}(t_k,x), \\ \alpha(t_{k+1}) = \alpha_0/(\mathrm{In}(e + \|\psi(t_{k+1},x) - \psi(t_k,x)\|), \end{cases}$$

where $\alpha(t_{k+1})(0 < \alpha(t_{k+1}) \leq 1)$ denotes the adaptive forgetting factor, starting with an initial value of α_0, which assigns weights to historical measurement data.

Remark 2.1. *Data accuracy is crucial for system performance and safety in control systems, with severe data distortion potentially causing system failure. The dynamic forgetting factor $\alpha(t_{k+1})$ in the ASSD mechanism assigns decay weights to historical measurements, smoothing sampling values and mitigating the impact of data distortion. A larger difference between the current and previous measurements results in a smaller forgetting factor $\alpha(t_{k+1})$, and vice versa. Furthermore, a larger deviation from the current measurement results in a smaller weight, while a smaller deviation leads to a larger weight. As $\tilde{\psi}(t_{k+1},x)$ is calculated iteratively, the ASSD mechanism requires storing only one historical data $\tilde{\psi}(t_t,x)$, thus utilizing less storage space compared to memory-based SD control [27]. When $\alpha(t_{k+1}) = 1$, the ASSD control simplifies to the conventional SD control outlined in [25, 26].*

Considering the effect of actuator saturation, the saturation function $\sigma(u(t,x))$ satisfies the following conditions:

$$\sigma(u(t,x)) = \sum_{j=1}^{\iota} \mathfrak{h}_j(\mathscr{C}(t_k))\sigma(\mathcal{K}_j\tilde{\psi}((t)_k,x)),\ t \in [t_k, t_{k+1}),$$

where $\sigma(u_i(t,x)) = sign(u_i(t,x))min\{\hat{u}_i(t,x), |u_i(t,x)|\}$ and $\hat{u}_i(t,x)$ represents the upper bound of the controller.

Furthermore, by defining $\varphi(\mathcal{K}_j\tilde{\psi}(t_k,x))$ as the dead-zone nonlinearity function, the saturation function $\sigma(u(t,x))$ is divided into two parts [28]:

$$\sigma(u(t,x)) = u(t,x) - \varphi(u(t,x)) = \sum_{j=1}^{\iota} \mathfrak{h}_j(\mathscr{C}(t_k))[\mathcal{K}_j\tilde{\psi}(t_k,x) - \varphi(\mathcal{K}_j\tilde{\psi}(t_k,x))], \tag{2.10}$$

and the following holds for a real number $\bar{\varphi}$ within the interval $(0,1)$:

$$\bar{\varphi}\tilde{\psi}^T(t_k,x)\mathcal{K}_j^T\mathcal{K}_j\tilde{\psi}(t_k,x) \geq \varphi^T(\mathcal{K}_j\tilde{\psi}(t_k,x))\varphi(\mathcal{K}_j\tilde{\psi}(t_k,x)). \tag{2.11}$$

Remark 2.2. *Actuator saturation is a critical factor that must be considered in controller design [28, 29]. Actuator saturation must be considered for two primary reasons: the physical limitations of the actuator and the impact of complex network conditions (such as external disturbances, packet loss, and delay) on system performance. To better capture the impact of actuator saturation, this paper models the saturation function $\sigma(u(t,x))$ as a combination of the linear segment $u(t,x)$ and the dead-zone nonlinear segment $\varphi(u(t,x))$, with their relationship defined in inequality (2.11). Additionally, the actuator saturation can be ignored when the saturation upper bound $\hat{u}_i(t,x)$ approaches infinity.*

By substituting the aforementioned equations into the error system (2.6), we obtain:

$$\frac{\partial\psi(t,x)}{\partial t} = \sum_{i=1}^{\iota}\sum_{j=1}^{\iota}\mathfrak{h}_i(\mathscr{C}(t))\mathfrak{h}_j(\mathscr{C}(t_k))\Big\{\sum_{l=1}^{m}\frac{\partial}{\partial x_l}(A_l\frac{\partial\psi(t,x)}{\partial x_l}) - B_i\psi(t,x) + C_ig(t,x) + D_ig(t-\sigma(t),x) + \mathcal{K}_j\tilde{\psi}(t_k,x) - \varphi(\mathcal{K}_j\tilde{\psi}(t_k,x))\Big\}. \tag{2.12}$$

Assumption 2.1. *[30] Assume that $\mathfrak{h}_p(\mathscr{C}(t))$ is a continuously differentiable function, and $\left|\dot{\mathfrak{h}}_p(\mathscr{C}(t))\right| \leq \lambda_p$ with $\lambda_p > 0$, $p \in N$.*

Lemma 2.1. *[31] If $\epsilon(x)$ is a continuously differentiable real-valued function defined on the set Γ and $\epsilon(x)/\partial\Gamma = 0$, then*

$$\int_{\Gamma}\varepsilon^2(x)ds \leq (\frac{\bar{\alpha}_l - \underline{\alpha}_l}{\pi})^2\int_{\Gamma}(\frac{\partial\varepsilon^2(x)}{\partial s_l})^2 ds,\ l = 1,2,...,m.$$

Lemma 2.2. *[32] Consider $\kappa(s)$ as the differentiable function mapping from $[r_1, r_2] \to R^n$. Given symmetric matrices $X \in R^{n\times n} > 0$ and matrices $N_1, N_2, \in R^{3n\times n}$, the subsequent inequality is satisfied:*

$$-\int_{r_1}^{r_2}\dot{\kappa}^T(s)X\dot{\kappa}(s)ds \leq \delta\vartheta^T(N_1X^{-1}N_1^T + \frac{1}{3}N_2X^{-1}N_2^T)\vartheta + \textbf{\textit{sym}}\left\{\vartheta^TN_1\Pi_1 + \vartheta^TN_2\Pi_2\right\},$$

where $\delta = r_2 - r_1$, $\vartheta = \left[\kappa^T(r_2)\ \kappa^T(r_1)\ \frac{1}{\delta}\int_{r_1}^{r_2}\kappa^T(s)ds\right]^T$, $\Pi_1 = \kappa^T(r_2) - \kappa^T(r_1)$ and $\Pi_2 = \kappa^T(r_2) + \kappa^T(r_1) - \frac{2}{\delta}\int_{r_1}^{r_2}\kappa^T(s)ds$.

3. Main results

For ease of presentation, the relevant notations are defined in Appendix A.

Theorem 3.1. *For given scalars $\bar{\sigma} > 0$, $\eth$, $\bar{\varphi}$, o_1, o_2, and controller gain matrix $\mathcal{K}_j$, the master–slave systems are asymptotically synchronized if there exist symmetric positive-definite matrices P_{1i}, P_{2i}, R_{1i}, R_{2i}, T_r, S, Λ_3, U_r, W_r, NA_l, positive-definite diagonal matrices Λ_r, appropriate dimensional matrices Y_q, H_p, G_p, M_q, N, where $r = 1,2$, $p = 1,2,3$, $q = 1,2,...,4$ and $i, j \in \mathbb{N}$, such that the following LMIs hold:*

$$\bar{\sigma}P_{2i} + G_1 \geq 0, \bar{\sigma}P_{1i} + G_1 \geq 0, \tag{3.1}$$

$$R_{1i} + G_2 \geq 0,\ R_{2i} + G_3 \geq 0, \tag{3.2}$$

$$\sum_{i=1}^{\iota}\lambda_i(R_{1i} + G_2) \leq (1-\eth)T_1, \tag{3.3}$$

$$\sum_{i=1}^{\iota}\lambda_i(R_{2i} + G_3) \leq T_2, \tag{3.4}$$

$$\begin{bmatrix}\mathfrak{U}[t_{k+1},\sigma(t)] & \sqrt{d_M}\Upsilon_1 \\ * & -\mathcal{U}_1\end{bmatrix} < 0,\ \sigma(t) \in \{0,\bar{\sigma}\}, \tag{3.5}$$

$$\begin{bmatrix} \mathfrak{N}[t_k, \sigma(t)] & \sqrt{d_M}\Upsilon_2 \\ * & -\mathcal{U}_2 \end{bmatrix} < 0,\ \sigma(t) \in \{0, \bar{\sigma}\}, \tag{3.6}$$

where the other notations are listed in Appendix B.

Proof.

$$V(t) = \begin{cases} \sum\limits_{\alpha=1}^{5} V_\alpha(t),\ t = t_k, \\ \sum\limits_{\beta=1}^{8} V_\beta(t),\ t \neq t_k, \end{cases} \tag{3.7}$$

where we choose LKFs candidates are defined in Appendix C. □

Next, taking the derivative of $V(t)$ for $t \in (t_k, t_{k+1})$ yields

$$\begin{aligned} \dot{V}(t) \leq & \int_\Gamma \zeta^T(t,x)\Sigma[t,\sigma(t)]\zeta(t,x)dx + \sum_{i=1}^{5} \mathfrak{Q}_i + 2\int_\Gamma \sum_{l=1}^{m} \frac{\partial^2 \psi^T(t,x)}{\partial x_l \partial t} N A_l \frac{\partial \psi(t,x)}{\partial x_l} dx \\ & - \int_\Gamma \int_{t_k}^{t} \frac{\partial \psi^T(s,x)}{\partial s} U_1 \frac{\partial \psi(s,x)}{\partial s} ds dx - \int_\Gamma \int_{t}^{t_{k+1}} \frac{\partial \psi^T(s,x)}{\partial s} U_2 \frac{\partial \psi(t,x)}{\partial s} ds dx. \end{aligned} \tag{3.8}$$

Considering the characteristic described in (2.4) and using symmetric TFRNN weighting matrices G_1, G_2, and G_3, the fuzzy zero equations are derived as follows:

$$\begin{cases} \int_\Gamma \psi^T(t,x) \sum\limits_{i=1}^{\iota} \dot{\mathfrak{b}}_i(C(t)) G_1 \psi(t,x) dx = 0, \\ \int_\Gamma \int_{t-\sigma(t)}^{t} \bar{\phi}^T(s,x) \sum\limits_{i=1}^{\iota} \dot{\mathfrak{b}}_i(C(t)) G_2 \bar{\phi}(s,x) ds dx = 0, \\ \int_\Gamma \int_{t-\bar{\sigma}}^{t} \psi^T(s,x) \sum\limits_{i=1}^{\iota} \dot{\mathfrak{b}}_i(C(t)) G_3 \psi(s,x) ds dx = 0. \end{cases}$$

For the fuzzy term $\mathfrak{Q}_1$ presented in Eq (3.8), given Assumption 2.1 and considering condition (3.1), it can be deduced that:

$$\mathfrak{Q}_1 + \int_\Gamma \psi^T(t,x) \sum_{i=1}^{\iota} \dot{\mathfrak{b}}_i(\mathscr{C}(t)) G_1 \psi(t,x) dx \leq \int_\Gamma \zeta^T(t,x)\Xi_1(t)\zeta(t,x)dx. \tag{3.9}$$

An analogous analysis applied to $\mathfrak{Q}_2$, $\mathfrak{Q}_3$, $\mathfrak{Q}_4$, and $\mathfrak{Q}_5$ in Eq (3.8) yields the following inequality from conditions (3.2)–(3.4):

$$\mathfrak{Q}_2 + \mathfrak{Q}_4 \leq \int_\Gamma \int_{t-\sigma(t)}^{t} \zeta^T(s,x)\Xi_2\zeta(s,x)ds dx \leq 0, \tag{3.10}$$

$$\mathfrak{Q}_3 + \mathfrak{Q}_5 \leq \int_\Gamma \int_{t-\sigma(t)}^{t} \zeta^T(s,x)\Xi_3\zeta(s,x)ds dx \leq 0. \tag{3.11}$$

By Lemma 2.2, processing the integral term in (3.8) yields the following inequality:

$$- \int_\Gamma \int_{t_k}^{t} \frac{\partial \psi^T(s,x)}{\partial s} U_1 \frac{\partial \psi(s,x)}{\partial s} ds$$

$$\leq \int_{\Gamma} \zeta^T(t,x)\Big(d_1(t)\Gamma_1\mathcal{U}_1^{-1}\Gamma_1^T + \mathbf{sym}\left\{\Phi_7^T M_1\Phi_4 + \Phi_7^T M_2\Phi_8\right\}\Big)\zeta(t,x)dx, \tag{3.12}$$

$$- \int_{\Gamma}\int_{t}^{t_{k+1}} \frac{\partial\psi^T(s,x)}{\partial s}U_2\frac{\partial\psi(s,x)}{\partial s}ds$$

$$\leq \int_{\Gamma} \zeta^T(t,x)\Big(d_2(t)\Gamma_2\mathcal{U}_2^{-1}\Gamma_2^T + \mathbf{sym}\left\{\Phi_9^T M_3\Phi_5 + \Phi_9^T M_4\Phi_{10}\right\}\Big)\zeta(t,x)dx, \tag{3.13}$$

where $\Upsilon_1 = [\Phi_7^T M_1\ \Phi_7^T M_2], \Upsilon_2 = [\Phi_9^T M_3\ \Phi_9^T M_4], \mathcal{U}_1 = \mathbf{diag}\{U_1, 3U_1\}, \mathcal{U}_2 = \mathbf{diag}\{U_2, 3U_2\}$.

Additionally, to improve the design flexibility of the proposed method, the matrix N and parameters o_1 and o_2 are introduced through the following equations:

$$\begin{aligned} 0 =& 2\int_{\Gamma}\mathcal{B}N\Big(\sum_{l=1}^{m}\frac{\partial}{\partial x_l}\Big(A_l\frac{\partial\psi(t,x)}{\partial x_l}\Big) - B_i\psi(t,x) + C_i g(t,x) \\ &+ D_i g(t-\sigma(t),x) + \mathcal{K}_j\tilde{\psi}(t_k,x) - \varphi(\mathcal{K}_j\tilde{\psi}(t_k,x)) - \frac{\partial\psi(t,x)}{\partial t}\Big)ds, \end{aligned} \tag{3.14}$$

where $\mathcal{B} = o_1\psi^T(t,x) + o_2\frac{\partial\psi^T(t,x)}{\partial t}$.

Using Green's formula and the specified boundary condition, the following equalities are established:

$$\begin{aligned} 2\int_{\Gamma}\frac{\partial\psi^T(t,x)}{\partial t}N\sum_{l=1}^{m}\frac{\partial}{\partial x_l}\left(A_l\frac{\partial\psi(t,x)}{\partial x_l}\right)dx =& 2\int_{\Gamma}\sum_{l=1}^{m}\frac{\partial}{\partial x_l}\left[\frac{\partial\psi^T(t,x)}{\partial t}NA_l\frac{\partial\psi(t,x)}{\partial x_l}\right]dx \\ &- 2\int_{\Gamma}\sum_{l=1}^{m}\frac{\partial^2\psi^T(t,x)}{\partial x_l\partial t}NA_l\frac{\partial\psi(t,x)}{\partial x_l}dx \\ =& -2\int_{\Gamma}\sum_{l=1}^{m}\frac{\partial^2\psi^T(t,x)}{\partial x_l\partial t}NA_l\frac{\partial\psi(t,x)}{\partial x_l}dx. \end{aligned} \tag{3.15}$$

Following the procedure in Eq (3.15) and applying Lemma 2.1, we obtain

$$\begin{aligned} 2\int_{\Gamma}\psi^T(t,x)N\sum_{l=1}^{m}\frac{\partial}{\partial x_l}\left(A_l\frac{\partial\psi(t,x)}{\partial x_l}\right)dx =& -2\int_{\Gamma}\sum_{l=1}^{m}\frac{\partial\psi^T(t,x)}{\partial x_l}NA_l\frac{\partial\psi(t,x)}{\partial x_l}dx \\ \leq& -2\int_{\Gamma}\psi^T(t,x)NA_\pi\psi(t,x)ds, \end{aligned} \tag{3.16}$$

where $A_\pi = \mathbf{diag}\left\{\sum_{l=1}^{\omega}(\frac{\pi}{\bar{\alpha}_l-\underline{\alpha}_l})^2A_{1l}, ..., \sum_{l=1}^{\omega}(\frac{\pi}{\bar{\alpha}_l-\underline{\alpha}_l})^2A_{nl}\right\}$.

From (2.7) and (2.11), it is clear that the following inequalities hold:

$$\begin{cases} -\int_{\Gamma}2\zeta^T(t,x)[\mathcal{E}_5 - \Omega_1\mathcal{E}_1]^T\Lambda_1[\mathcal{E}_5 - \Omega_2\mathcal{E}_1]\zeta(t,x)dx \geq 0, \\ -\int_{\Gamma}2\zeta^T(t,x)[\mathcal{E}_6 - \Omega_1\mathcal{E}_3]^T\Lambda_2[\mathcal{E}_6 - \Omega_2\mathcal{E}_3]\zeta(t,x)dx \geq 0, \\ \int_{\Gamma}2\zeta^T(t,x)[\bar{\varphi}\mathcal{E}_{12}^T\mathcal{K}_j^T\Lambda_3\mathcal{K}_j\mathcal{E}_{12} - \mathcal{E}_{13}^T\Lambda_3\mathcal{E}_{13}]\zeta(t,x)dx \geq 0. \end{cases} \tag{3.17}$$

Combining (3.8)–(3.17), we deduce

$$\dot{V}(t) \leq \int_{\Gamma}\zeta^T(t,x)\mathfrak{G}(t,\sigma(t))\zeta^T(t,x)dx, \tag{3.18}$$

where $\mathfrak{G}[t,\sigma(t)] = \sum_{i=1}^{\iota}\sum_{j=1}^{\iota}\mathfrak{h}_i(\mathscr{C}(t))\mathfrak{h}_j(\mathscr{C}(t_k))\mathfrak{C}[t,\sigma(t)] + d_1(t)\Upsilon_1\mathcal{U}_1^{-1}\Upsilon_1^T + d_2(t)\Upsilon_2\mathcal{U}_2^{-1}\Upsilon_2^T$.

In addition, from $V_6(t_k^+) = V_7(t_{k+1}^-) = 0$ and $\sum_{\alpha=1}^{5} V_\alpha(t)$ being continuous, we can obtain

$$\Big(V(t_{k+1}^-) - \sum_{\alpha=1}^{5} V_\alpha(t_{k+1})\Big) - \Big(V(t_k^+) - \sum_{\alpha=1}^{5} V_\alpha(t_k)\Big) = V_6(t_{k+1}^-) - V_7(t_k^+) \geq d_M \int_\Gamma \zeta^T(t,x)\mathfrak{F}\zeta(t,x)dx. \quad (3.19)$$

Based on the methodology in reference [33] and the condition $\mathfrak{A}[t,\sigma(t)] = \mathfrak{C}[t,\sigma(t)] - \mathfrak{F} < 0$, the following inequality holds:

$$d_k\dot{V}(t) \leq V_6(t_{k+1}^-) - V_7(t_k^+). \quad (3.20)$$

By employing the Schur complement, the inequality $\mathfrak{A}[t,\sigma(t)] < 0$ remains valid for $t \in (t_k, t_{k+1})$ and $\sigma(t) \in [0,\bar{\sigma}]$ given that it satisfy (3.5) and (3.6).

Remark 3.1. *By introducing LKF, $V_4(t) = \int_\Gamma (t_{k+1} - t)\tilde{\psi}^T(t_k,x)\, S\tilde{\psi}(t_k,x)dx$, we obtain $\dot{V}_4(t) = -\int_\Gamma \zeta^T(t,x)\mathcal{E}_{12}^T S\mathcal{E}_{12}\zeta(t,x)dx$, which leads to the sufficient condition in Theorem 3.1 for synchronizing the master–slave system. The primary purpose of $V_4(t)$ is to facilitate finding a solution to the feasible LMIs. Removing $V_4(t)$ renders the LMIs in Theorem 3.1 infeasible, as it sets the matrix diagonal element $-\mathcal{E}_{12}^T S\mathcal{E}_{12}$ to zero. Consequently, without $V_4(t)$, the synchronization of the master–slave system under ASSD control cannot be guaranteed.*

Remark 3.2. *Based on prior experience, capturing more system information in the constructed LKF yields less conservative results. To achieve the larger MASI, $V_1(t)$ and $V_2(t)$ incorporate the properties of the membership function and the time-varying delays. $V_5(t)$,$V_6(t)$, and $V_7(t)$ consider more detailed system state information at the sampling point. In addition, when $P_{1n} = P_{2m}$ $(n,m \in \mathbb{N})$ holds, LKF $V_1(t)$ simplifies to the basic quadratic form $\int_\Gamma e^T(t,x)Pe(t,x)dx$ [21, 26].*

Remark 3.3. *The integral terms $\mathfrak{Q}_1$ and $\mathfrak{Q}_2$, which are related to the derivatives of the membership function, are handled using the fuzzy zero equations and the compensation LKF method. First, by using the membership function's property in (2.4), fuzzy zero equations are applied to introduce additional TFRNN-weighting matrices via matrices G_2 and G_3. Then, the compensation LKF $V_3(t)$ introduces the integral terms $\mathfrak{Q}_4$ and $\mathfrak{Q}_5$, which are independent of tcompensation LKF relaxed the initial constraints of the membership function. Finally, the fuzzy zero equation and $\sum_{i=1}^{\iota}\lambda_i(R_{1i}+G_2) \leq 0$ and $\sum_{i=1}^{\iota}\lambda_i(R_{2i}+G_3) \leq 0$ to conditions (3.4) and (3.5).*

Remark 3.4. *The looped-functional method is commonly used to reduce conservatism in SD control [24, 34, 35]. The advantage of this method is that it does not require the restriction matrix to be positive definite in function but ensures that $V_l(t_k) = V_l(t_{k+1}) = 0$ at the terminal points of the sampling interval. The semi-looped-functional method improves upon the looped-functional method. In this paper, the terms $V_6(t)$ and $V_7(t)$ are referred to as semi-looped-functionals because $V_6(t_k^+) = 0, V_6(t_{k+1}^-) \neq 0$ and $V_7(t_k^+) \neq 0, V_7(t_{k+1}^-) = 0$. Therefore, semi-looped-functionals offer more flexibility than looped-functionals. In contrast, the sum of the derivatives of LKFs is typically required to be negative definite in the traditional LKF approach [13, 17, 21, 24]. The discontinuities of semi-looped-functionals enable the removal of the negative definite restriction. We ensure that $\dot{V}(t)$ meets*

the condition $d_M\dot{V}(t) \le V_6(t_{k+1}^-) - V_7(t_k^+)$, resulting in $V(t_k) > V(t_{k+1})$. It is evident that the semi-looped-functional method has more relaxed constraints and thus results in less conservative outcomes.

Corollary 3.1. *For given scalars $\bar{\sigma} > 0$, $\eth$, $\ni$, $\bar{\varphi}$, o_1, and o_2, the master–slave systems are asymptotically synchronized if there exist symmetric positive-definite matrices P_{1i}, P_{2i}, R_{1i}, R_{2i}, T_r, S, Λ_3, U_r, W_r, NA_l, positive-definite diagonal matrices Λ_r; and appropriate dimensional matrices Y_q, H_p, G_p, M_q, N, $\hat{N}_r$, where $r = 1, 2$, $p = 1, 2, 3$, $q = 1, 2, ..., 4$ and $i, j \in \mathbb{N}$, such that the following LMIs hold:*

$$\bar{\sigma}P_{2i} + G_1 \ge 0,\ \bar{\sigma}P_{1i} + G_1 \ge 0, \tag{3.21}$$

$$R_{1i} + G_2 \ge 0,\ R_{2i} + G_3 \ge 0, \tag{3.22}$$

$$\sum_{i=1}^{\iota} \lambda_i(R_{1i} + G_2) \le (1 - \eth)T_1, \tag{3.23}$$

$$\sum_{i=1}^{\iota} \lambda_i(R_{2i} + G_3) \le T_2, \tag{3.24}$$

$$\begin{bmatrix} \mathfrak{U}_{ij}^*[t_{k+1}, \sigma(t)] & \sqrt{d_k}\Upsilon_1 & \mathfrak{J}_j^{13} \\ * & -\mathcal{U}_1 & 0_n \\ * & * & \mathfrak{J}_j^{33} \end{bmatrix} < 0,\ \sigma(t) \in \{0, \bar{\sigma}\}, \tag{3.25}$$

$$\begin{bmatrix} \mathfrak{U}_{ij}^*[t_k, \sigma(t)] & \sqrt{d_k}\Upsilon_2 & \mathfrak{J}_j^{13} \\ * & -\mathcal{U}_2 & 0_n \\ * & * & \mathfrak{J}_j^{33} \end{bmatrix} < 0,\ \sigma(t) \in \{0, \bar{\sigma}\}, \tag{3.26}$$

where the relevant notations are given as follows:

$$\begin{aligned} \mathfrak{C}^*[t, \sigma(t)] =& \Sigma[t, \sigma(t)] + \Xi_1(t) + \boldsymbol{sym}\{-\mathcal{E}_1^T NA_\pi \mathcal{E}_1 - [\mathcal{E}_5 - \Omega_1\mathcal{E}_1]^T \Lambda_1 [\mathcal{E}_5 - \Omega_2\mathcal{E}_1] \\ & - [\mathcal{E}_6 - \Omega_1\mathcal{E}_3]^T \Lambda_2 \times [\mathcal{E}_6 - \Omega_2\mathcal{E}_3] - \mathcal{E}_{13}^T \Lambda_3 \mathcal{E}_{13} \\ & + (o_1\mathcal{E}_1^T + o_2\mathcal{E}_2^T)(N(-B_i\mathcal{E}_1 + C_i\mathcal{E}_5 + D_i\mathcal{E}_6 - \mathcal{E}_{13} - \mathcal{E}_2) + \hat{N}_j\mathcal{E}_{12}) \\ & + \Phi_7^T M_1 \Phi_4 + \Phi_7^T M_2 \Phi_8 + \Phi_9^T M_3 \Phi_5 + \Phi_9^T M_4 \Phi_{10}\}, \\ \mathfrak{U}^*[t, \sigma(t)] =& \mathfrak{C}^*[t, \sigma(t)] - \mathfrak{F},\ \mathfrak{J}_j^{33} = -2\ni_1\hat{N}_j + \ni_1^2\,\bar{\varphi}\Lambda_3,\ \mathfrak{J}_j^{13} = \Big[\underbrace{0_n, ..., 0_n}_{11}, \hat{N}_j^T\ 0_n\Big]^T, \end{aligned}$$

and the controller gains are given as follows:

$$\mathcal{K}_j = N^{-1}\hat{N}_j. \tag{3.27}$$

Proof. To address this within the LMI framework, the nonlinear component of Theorem 3.1 has been linearized as described in Corollary 3.1. Conducting a congruence transformation using

$$\mathbf{diag}\{\underbrace{I_n, ..., I_n}_{15}, N_j\} \text{ and } \mathbf{diag}\{\underbrace{I_n, ..., I_n}_{15}, N_j\}$$

into (3.5) and (3.6), substituting $\hat{N}_j = N\mathcal{K}_j$ and $-\bar{\varphi}\hat{N}_j\Lambda_3^{-1}\hat{N}_j \le -2\ni_1\hat{N}_j + \ni_1^2\,\bar{\varphi}\Lambda_3$ one obtains (3.25) and (3.26). This completes the proof. □

4. Simulation results

Example 4.1. *Consider system parameters of the TFRNNs as follows [26]:*

$$A_l = \begin{bmatrix} 0.6 & 0 \\ 0 & 0.6 \end{bmatrix}, B_1 = \begin{bmatrix} 1 & 0 \\ 0 & 1 \end{bmatrix}, C_1 = \begin{bmatrix} 2 & -0.1 \\ -5 & 3 \end{bmatrix}, D_1 = \begin{bmatrix} -1.5 & -0.1 \\ -0.2 & -2.5 \end{bmatrix}, B_2 = \begin{bmatrix} 1.2 & 0 \\ 0 & 1.2 \end{bmatrix},$$

$$C_2 = \begin{bmatrix} 3.6 & -0.4 \\ -8 & 8 \end{bmatrix}, D_2 = \begin{bmatrix} -3.6 & -0.24 \\ -0.6 & -6 \end{bmatrix}, \underline{\alpha}_l = -1, \overline{\alpha}_l = 5, \sigma(t) = \left| \sqrt{2} \sin(0.1t + \frac{\pi}{4}) \right|,$$

$$\mathfrak{T}(t) = 0, \ g(t,x) = tanh(\varsigma(t,x)) - tanh(\bar{\varsigma}(t,x)), \ \mathfrak{h}_1(\mathscr{C}(t)) = 0.5 + 0.5\sin t, \mathfrak{h}_2(\mathscr{C}(t)) = 0.5 - 0.5\sin t.$$

From these conditions, we deduce that $\bar{\sigma} = \sqrt{2}$, $\mathfrak{d} = \frac{\sqrt{2}}{10}$, $\Omega_1 = 0_2$, and $\Gamma_2 = I_2$. For the master system (2.3), the initial conditions are set as $\mathfrak{g}_1(s,x) = 1.5\rho(x)$ and $\mathfrak{g}_2(s,x) = -2\rho(x)$. For the slave system (2.5), the initial conditions are defined as $\bar{\mathfrak{g}}_1(s,x) = 1.425\rho(x)$ and $\bar{\mathfrak{g}}_2(s,x) = -2.1\rho(x)$, where $\rho(x) = \cos\left(\frac{\pi(x-2)}{6}\right)$.

This paper employs three-dimensional surface plots to visually represent the system's state trajectories across time and space. These plots feature the spatial variable x and the time variable t as independent variables, with the system state value $\psi_i(t,x)$ as the dependent variable. When $u(t,x) = 0$, Figure 1 shows the trajectories of states $\psi_i(t,x)$ and $\|\psi(t,x)\|$. Figure 1(a) and (b) show that the surface fluctuates continuously, indicating that the system state trajectories oscillate across the entire spatial range. Additionally, Figure 1(c) shows the evolution of $\|\psi(t,x)\|$. It quantitatively represents the synchronization error, showing how close or far the master–slave system is from the desired state. A smaller error value indicates a higher level of synchronization between the master–slave system. From Figure 1(c), the $\|\psi(t,x)\|$ is divergent and cannot converge to 0. In summary, this implies that the TFSRDNN master–slave system cannot achieve synchronization without ASSD control inputs.

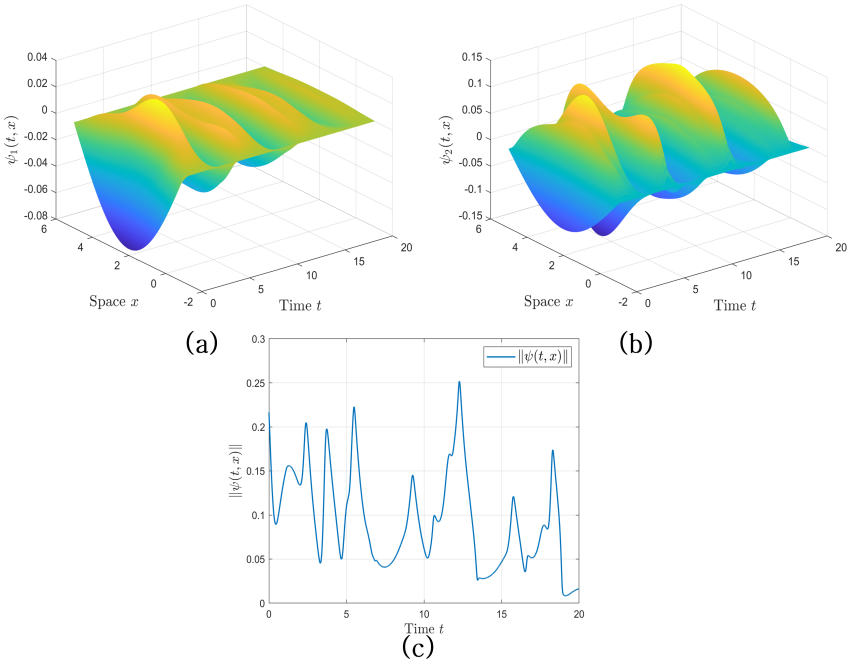

Figure 1. Trajectories of states without control input. (a) $\psi_1(t,x)$. (b) $\psi_2(t,x)$. (c) $\|\psi(t,x)\|$.

Using Algorithm 1 and the solving parameters $o_1 = -0.1943$ and $o_2 = 0.4210$, we obtain the MASI $d_M = 0.0767$. Utilizing the matrix relations presented in (3.27), the corresponding controller gains are solved as $\mathcal{K}_1 = \mathcal{K}_2 = [-6.9728 \quad -2.9979; 3.0663 \quad -6.8996]$. We then analyzed the system's motion trajectory images to evaluate the controller's effectiveness. Figure 2 illustrates the controlled trajectories of states $\psi_i(t, x)$ and $\|\psi(t, x)\|$ using these controller gains. Figure 2(a) and (b) show the original fluctuating surface gradually becoming the plane at $\psi_i(t, x) = 0$. In simpler terms, the system's states $\psi_i(t, x)$ approach 0 across all spatial dimensions. Figure 3(c) depicts the evolution of the controlled $\|\psi(t, x)\|$, demonstrating its rapid convergence under ASSD control inputs. Notably, around $t = 2$, $\|\psi(t, x)\|$ reaches 0 and is not fluctuating. Comparing Figures 1 and 2 shows that the ASSD controller and Corollary 3.1, as designed in this paper, effectively synchronize the master–slave system.

Algorithm 1: *Solve the upper bound of the MASI.*

Input: $\bar{\sigma}$, ð, ə, $\bar{\varphi}$, o_1, o_2, d_1
Output: *Maximum* d_M

```
1  begin
2      Solve LMIs (3.21)-(3.26)
3      if there is no solution then
4          go to Line 8
5      else
6          go to Line 15
7      end
8      for T_a = 0 : 0.0001 : 1 do
9          k = fix(T_a × 10^4) and d_{k+1} ← d_k + T_a
10         Solve LMIs (32)-(38)
11         if there is no solution then
12             Save d_M ← d_k and break
13         end
14     end
15     for T_b = 0 : 0.0001 : 1 do
16         k = fix(T_b × 10^4) and d_{k+1} ← d_k − T_b
17         Solve LMIs (32)-(38)
18         if there is solution then
19             Save d_M ← d_{k+1} and break
20         end
21     end
22 end
```

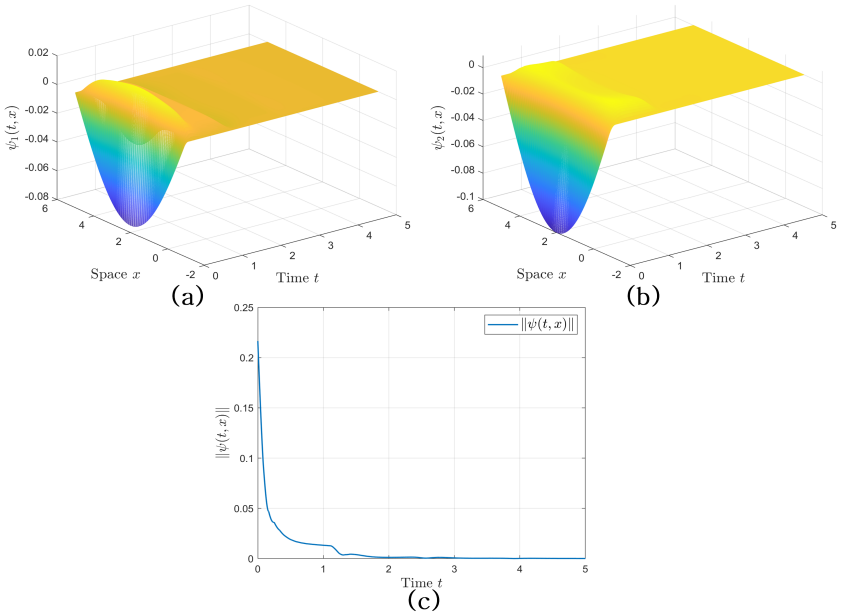

Figure 2. Trajectories of controlled states and the corresponding ASSD control input. (a) $\psi_1(t,x)$; (b) $\psi_2(t,x)$. (c)$\|\psi(t,x)\|$.

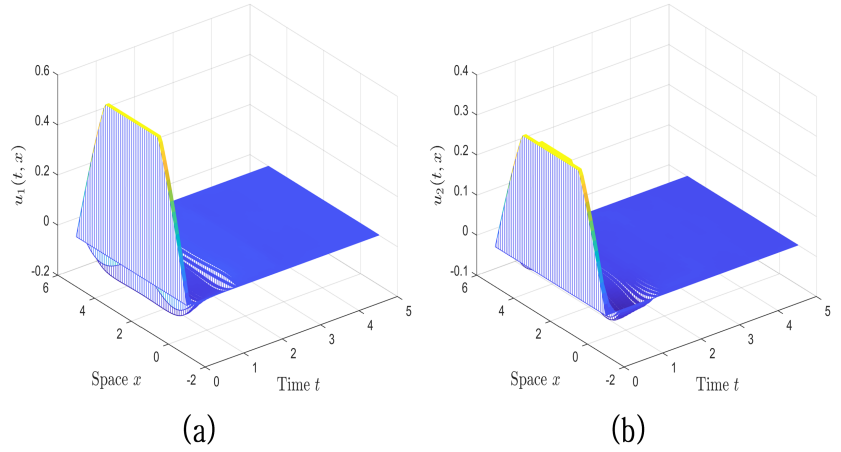

Figure 3. Trajectories of ASSD control input. (a) $u_1(t,x)$; (b) $u_2(t,x)$.

To demonstrate the ASSD controller's effectiveness in complex real-world scenarios, we examine actuator saturation. Figure 3(a) and (b) illustrate the effects of actuator saturation on control inputs. At $u_1(t,x) = 0.60$ and $u_2(t,x) = 0.32$, the originally curved boundary transitions to a straight one. This indicates that the saturation upper limits are 0.60 and 0.32, respectively. The ASSD controller effectively synchronizes the master–slave system, even under actuator saturation, demonstrating its reliability.

In SD control, MASI is a key performance indicator. A larger MASI indicates the use of fewer communication resources to achieve the desired control effect. Table 2 compares the MASI values for Corollary 3.1 in this paper with those of existing methods, highlighting the superiority of our method.

Under identical conditions, Corollary 3.1 in this paper is less conservative. It achieves the 12.2% and 35.9% improvement in MASI values compared with Corollary 1 [26] and Theorem 1 [26], which MASI values are 0.0683 and 0.0564, respectively.

Table 2. MASIs d_M in different methods.

Method	MASI d_M	Increased
Corollary 3.1	0.0767	–
Corollary 1 [26]	0.0683	12.2%
Theorem 1 [26]	0.0564	35.9%

Example 4.2. *Consider the TFRNNs with the following parameters:*

$$A_l = \begin{bmatrix} 0.8 & 0 \\ 0 & 0.8 \end{bmatrix},\ B_1 = \begin{bmatrix} 0.9 & 0 \\ 0 & 0.9 \end{bmatrix},\ C_1 = \begin{bmatrix} 2.2 & -0.11 \\ -5.5 & 3.3 \end{bmatrix},\ D_1 = \begin{bmatrix} -1.65 & -0.11 \\ -0.22 & -2.75 \end{bmatrix},\ B_2 = \begin{bmatrix} 1.8 & 0 \\ 0 & 1.8 \end{bmatrix},$$
$$C_2 = \begin{bmatrix} 4.4 & -0.22 \\ -6.6 & 6.6 \end{bmatrix}, D_2 = \begin{bmatrix} -3.1 & -0.22 \\ -0.44 & -5.2 \end{bmatrix},\ \underline{\alpha}_l = 0, \overline{\alpha}_l = 6,\ \sigma(t) = \frac{2e^t - 2}{2 + e^t}, \mathfrak{T}(t) = 0,$$
$$\mathfrak{h}_1(\mathscr{C}(t)) = 0.9(1 + 0.1\sin t), \mathfrak{h}_2(\mathscr{C}(t)) = 0.1(1 - 0.9\sin t),\ g(t, x) = tanh(\varsigma(t, x)) - tanh(\bar{\varsigma}(t, x)),$$

from which we obtain $\bar{\sigma} = 2$, $\eth = 4/9$, $\Omega_1 = 0_2$, *and* $\Omega_2 = I_2$. *For the master system (2.3), set initial conditions as* $\mathfrak{g}_1(s, x) = 2.8\rho(x)$ *and* $\mathfrak{g}_2(s, x) = -1.3\rho(x)$. *For the slave system (2.5), set them as* $\bar{\mathfrak{g}}_1(s, x) = 2.7\rho(x)$ *and* $\bar{\mathfrak{g}}_2(s, x) = -1.4\rho(x)$, *and* $\rho(x) = \cos(\pi x)$.

For $u(t, x) = 0$, Figure 4 illustrates the trajectories of states $\psi_i(t, x)$ and $\|\psi(t, x)\|$. Observations from Figure 4(a) and (b) reveal that the system's state continuously oscillates. Furthermore, Figure 4(c) indicates that $\|\psi(t, x)\|$ never converges to 0. This means that without control inputs, the master-slave system cannot achieve synchronization. Based on Algorithm 1 and the choice of solving parameters $o_1 = -2.4019$ and $o_2 = -1.9352$, we can obtain the MASI $d_M = 0.2753$. Utilizing the matrix relations presented in (3.27), the corresponding controller gains are solved as $\mathcal{K}_1 = \mathcal{K}_2 = [-1.8731\ 0.2639; 0.4181\ -3.3359]$. Figure 5 shows the controlled trajectories of states $\psi_i(t, x)$ and $\|\psi(t, x)\|$ using these controller gains. Figure 5(a) and (b) illustrate that the system state effectively converges to 0 under ASSD control. In Figure 5(c), the $\|\psi(t, x)\|$ rapidly converges to 0 after control is applied, around $t = 5$. The master–slave system achieves synchronization in Figure 5, demonstrating the effectiveness of Corollary 3.1 and the ASSD controller. Figure 6(a) and (b) show the impact of actuator saturation on control inputs. These reveal that actuator saturation affects control input values, setting upper limits at 0.10 and 0.20.

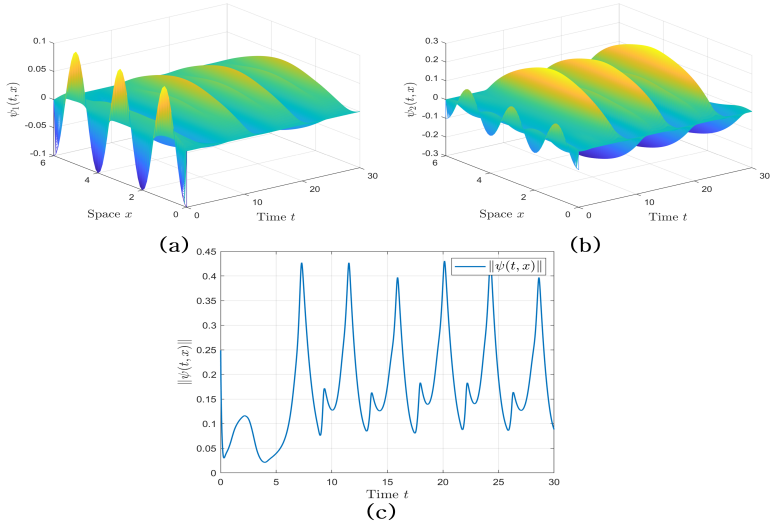

Figure 4. Trajectories of states without control input. (a) $\psi_1(t,x)$; (b) $\psi_2(t,x)$; (c) $\|\psi(t,x)\|$.

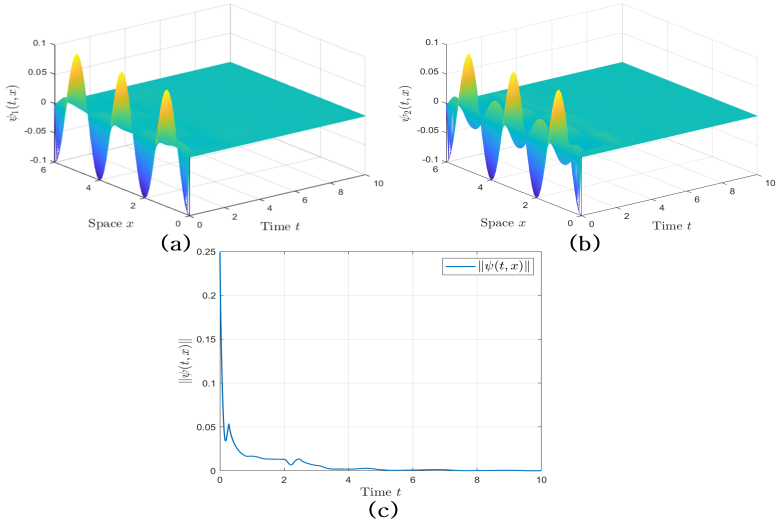

Figure 5. Trajectories of controlled states and the corresponding ASSD control input. (a) $\psi_1(t,x)$; (b) $\psi_2(t,x)$; (c)$\|\psi(t,x)\|$.

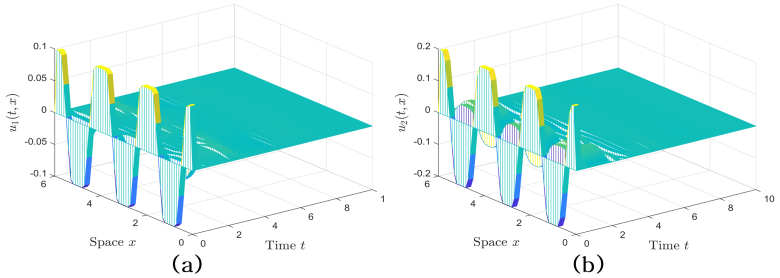

Figure 6. Trajectories of ASSD control input. (a) $u_1(t,x)$; (b) $u_2(t,x)$.

5. Conclusions

The synchronization issue of TFRNNs with time-varying delays and actuator saturation has been investigated. Then, the ASSD controller has been utilized for synchronization to conserve communication resources and enhance system resilience. Subsequently, we have constructed the LKFs that incorporate more system information. Moreover, fuzzy zero equations and compensation LKF have been used to handle terms with derivatives of the membership function, relaxing the constraints. The semi-looped-functional terms have been constructed to enlarge the feasible space further. Furthermore, sufficient conditions for synchronizing TFRNNs and a search algorithm for MASI have been established. Finally, two simulations have been exemplified to demonstrate the approach's feasibility.

Author contributions

Yuchen Niu: Investigation, software, validation, writing – original draft; Kaibo Shi: Conceptualization, writing – review & editing; Xiao Cai: Data curation, writing – review & editing; Shiping Wen: Writing – review & editing. All authors have read and approved the final version of the manuscript for publication.

Use of Generative-AI tools declaration

The authors declare that they have not used Artificial Intelligence (AI) tools in the creation of this article.

Conflict of interest

The authors declare that there are no conflicts of interest.

References

1. X. Sun, L. Zhang, J. Gu, Neural-network based adaptive sliding mode control for Takagi–Sugeno fuzzy systems, *Inform. Sci.*, **628** (2023), 240–253. https://doi.org/10.1016/j.ins.2022.12.118
2. X. Cai, K. Shi, Y. Sun, J. Cao, S. Wen, Z. Tian, Intelligent event-triggered control supervised by mini-batch machine learning and data compression mechanism for TS fuzzy NCSs under DoS attacks, *IEEE Trans. Fuzzy Syst.*, **32** (2023), 804–815. https://doi.org/10.1109/TFUZZ.2023.3308933
3. T. Gao, X. Bai, C. Wang, L. Zhang, J. Zheng, J. Wang, A modified interval type-2 Takagi–Sugeno fuzzy neural network and its convergence analysis, *Pattern Recogn.*, **131** (2022), 108861. https://doi.org/10.1016/j.patcog.2022.108861
4. A. Salimi-Badr, M. M. Ebadzadeh, A novel learning algorithm based on computing the rules' desired outputs of a TSK fuzzy neural network with non-separable fuzzy rules, *Neurocomputing*, **470** (2022), 139–153. https://doi.org/10.1016/j.neucom.2021.10.103

5. J. Liu, T. Yin, X. Xie, E. Tian, S. Fei, Event-triggered state estimation for T–S fuzzy neural networks with stochastic cyber-attacks, *Int. J. Fuzzy Syst.*, **21** (2019), 532–544. https://doi.org/10.1007/s40815-018-0590-4
6. Z. Cai, L. Huang, Z. Wang, Particular-function-based preassigned-time stability of discontinuous system: Novel control scheme for fuzzy neural networks, *IEEE Trans. Fuzzy Syst.*, **31** (2023), 1020-1030. https://doi.org/10.1109/TFUZZ.2022.3193759
7. K. Shi, J. Wang, Y. Tang, S. Zhong, Reliable asynchronous sampled-data filtering of T–S fuzzy uncertain delayed neural networks with stochastic switched topologies, *Fuzzy Sets Syst.*, **381** (2020), 1–25. https://doi.org/10.1016/j.fss.2018.11.017
8. X. Cai, K. Shi, Y. Sun, J. Cao, S. Wen, C. Qiao, et al., Stability analysis of networked control systems under DoS attacks and security controller design with mini-batch machine learning supervision, *IEEE Trans. Inf. Foren. Sec.*, **19** (2023), 3857–3865. https://doi.org/10.1109/TIFS.2023.3347889
9. C. Zhang, H. Wu, X. Han, X. Zhang, Exponential synchronization of reaction-diffusion neural networks via switched event-triggered control, *Inf. Sci.*, **648** (2023), 119599. https://doi.org/10.1016/j.ins.2023.119599
10. S. Lin, X. Liu, Synchronization and control for directly coupled reaction-diffusion neural networks with multiple weights and hybrid coupling, *Neurocomputing*, **487** (2022), 144–156. https://doi.org/10.1016/j.neucom.2022.02.061
11. D. Tong, B. Ma, Q. Chen, Y. Wei, P. Shi, Finite-time synchronization and energy consumption prediction for multilayer fractional-order networks, *IEEE Trans. Circuits Syst. II. Express Briefs*, **70** (2023), 2176–2180. https://doi.org/10.1109/TCSII.2022.3233420
12. M. Shi, D. Tong, Q. Chen, W. Zhou, Pth moment exponential synchronization for delayed multi-agent systems with Lévy noise and Markov switching, *IEEE Trans. Circuits Syst. II. Express Briefs*, **71** (2024), 697–701. https://doi.org/10.1109/TCSII.2023.3304635
13. S. Yan, Z. Gu, J. H. Park, X. Xie, Synchronization of delayed fuzzy neural networks with probabilistic communication delay and its application to image encryption, *IEEE Trans. Fuzzy Syst.*, **31** (2023), 930–940. https://doi.org/10.1109/TFUZZ.2022.3193757
14. X. W. Zhang, H. N. Wu, J. L. Wang, Z. Liu, R. Li, Membership-function-dependent fuzzy control of reaction-diffusion memristive neural networks with a finite number of actuators and sensors, *Neurocomputing*, **514** (2022), 94–100. https://doi.org/10.1016/j.neucom.2022.09.126
15. X. Yang, Q. Song, J. Cao, J. Lu, Synchronization of coupled Markovian reaction-diffusion neural networks with proportional delays via quantized control, *IEEE Trans. Neural Netw. Learn. Syst.*, **30** (2019), 951–958. https://doi.org/10.1109/TNNLS.2018.2853650
16. R. Zhang, D. Zeng, J. H. Park, H. K. Lam, S. Zhong, Fuzzy adaptive event-triggered sampled-data control for stabilization of T–S fuzzy memristive neural networks with reaction-diffusion terms, *IEEE Trans. Fuzzy Syst.*, **29** (2021), 1775–1785. https://doi.org/10.1109/TFUZZ.2020.2985334
17. X. M. Zhang, Q. L. Han, X. Ge, A novel approach to H_∞ performance analysis of discrete-time networked systems subject to network-induced delays and malicious packet dropouts, *Automatica*, **136** (2022), 110010. https://doi.org/10.1016/j.automatica.2021.110010
18. S. Gong, Z. Guo, S. Wen, Finite-time synchronization of T–S fuzzy memristive neural networks with time delay, *Fuzzy Sets Syst.*, **459** (2023), 67–81. https://doi.org/10.1016/j.fss.2022.10.013

19. H. Li, C. Li, D. Ouyang, S. K. Nguang, Z. He, Observer-based dissipativity control for T–S fuzzy neural networks with distributed time-varying delays, *IEEE Trans. Cybern.*, **51** (2021), 5248–5258. https://doi.org/10.1109/TCYB.2020.2977682

20. X. Li, T. Huang, J. A. Fang, Event-triggered stabilization for Takagi–Sugeno fuzzy complex-valued memristive neural networks with mixed time-varying delays, *IEEE Trans. Fuzzy Syst.*, **29** (2021), 1853–1863. https://doi.org/10.1109/TFUZZ.2020.2986713

21. F. Fang, Y. Liu, J. H. Park, Y. Liu, Outlier-resistant nonfragile control of T–S fuzzy neural networks with reaction-diffusion terms and its application in image secure communication, *IEEE Trans. Fuzzy Syst.*, **31** (2023), 2929–2942. https://doi.org/10.1109/TFUZZ.2023.3239732

22. Y. Liu, F. Fang, J. Zhou, Y. Liu, H_∞ state estimation for T–S fuzzy reaction-diffusion delayed neural networks with randomly occurring gain uncertainties and semi-Markov jump parameters, *Neurocomputing*, **493** (2022), 385–396. https://doi.org/10.1016/j.neucom.2022.04.060

23. X. Cai, K. Shi, K. She, S. Zhong, Y. Soh, Y. Yu, Performance degradation estimation mechanisms for networked control systems under DoS attacks and its application to autonomous ground vehicle, *IEEE Trans. Cybern.*, **54** (2024), 2992–3002. https://doi.org/10.1109/TCYB.2023.3286878

24. W. Ji, J. Qiu, H. K. Lam, A new sampled-data output-feedback controller design of nonlinear systems via fuzzy affine models, *IEEE Trans. Cybern.*, **52** (2022), 1681–1690. https://doi.org/10.1109/TCYB.2020.2984331

25. Z. You, H. Yan, H. Zhang, M. Wang, K. Shi, Sampled-data control for exponential synchronization of delayed inertial neural networks with aperiodic sampling and state quantization, *IEEE Trans. Neural Netw. Learn. Syst.*, **35** (2024), 5079–5091. https://doi.org/10.1109/TNNLS.2022.3202343

26. R. Zhang, D. Zeng, J. H. Park, H. K. Lam, X. Xie, Fuzzy sampled-data control for synchronization of T–S fuzzy reaction–diffusion neural networks with additive time-varying delays, *IEEE Trans. Cybern.*, **51** (2020), 2384–2397. https://doi.org/10.1109/TCYB.2020.2996619

27. S. Wang, K. Shi, J. Wang, Y. Yu, S. Wen, J. Yang, et al., Synchronization sampled-data control of uncertain neural networks under an asymmetric Lyapunov–Krasovskii functional method, *Expert Syst. Appl.*, **239** (2023), 122475. https://doi.org/10.1016/j.eswa.2023.122475

28. L. Sun, Y. Wang, G. Feng, Control design for a class of affine nonlinear descriptor systems with actuator saturation, *IEEE Trans. Autom. Control*, **60** (2015), 2195–2200. https://doi.org/10.1109/TAC.2014.2374712

29. H. Lu, Y. Deng, W. Zhou, Adaptive event-triggered H_∞ control for networked control systems with actuator saturation and random nonlinearities, *IEEE Access*, **8** (2020), 220723–220733. https://doi.org/10.1109/ACCESS.2020.3043337

30. Y. Li, Y. He, Y. Yang, Stability analysis for delayed T–S fuzzy systems: A compensation Lyapunov-Krasovskii functional method combined with free-weighting matrices, *ISA Trans.*, **142** (2023), 12–19. https://doi.org/10.1016/j.isatra.2023.08.020

31. J. Zhou, S. Xu, B. Zhang, Y. Zou, H. Shen, Robust exponential stability of uncertain stochastic neural networks with distributed delays and reaction-diffusions, *IEEE Trans. Neural Netw. Learn. Syst.*, **23** (2012), 1407–1416. https://doi.org/10.1109/TNNLS.2012.2203360

32. A. Seuret, F. Gouaisbaut, Wirtinger-based integral inequality: Application to time-delay systems, *Automatica*, **49** (2013), 2860–2866. https://doi.org/10.1016/j.automatica.2013.05.030

33. Z. Sheng, C. Lin, S. Xu, A semi-looped-functional for stability analysis of sampled-data systems, *IEEE/CAA J. Automat. Sinica*, **10** (2023), 1332–1335. https://doi.org/10.1109/JAS.2023.123498
34. H. B. Zeng, K. L. Teo, Y. He, A new looped-functional for stability analysis of sampled-data systems, *Automatica*, **82** (2017), 328–331. https://doi.org/10.1016/j.automatica.2017.04.051
35. H. B. Zeng, K. L. Teo, Y. He, H. Xu, W. Wang, Sampled-data synchronization control for chaotic neural networks subject to actuator saturation, *Neurocomputing*, **260** (2017), 25–31. https://doi.org/10.1016/j.neucom.2017.02.063

A. Appendix-A

$$\zeta(t,x)=\Big[\psi^T(t,x)\ \frac{\partial\psi^T(t,x)}{\partial t}\ \psi^T(t-\sigma(t),x)\ \psi^T(t-\bar{\sigma},x)\ g^T(t,x)\ g^T(t-\sigma(t),x)\ \phi_0^T(x)\ \phi_1^T(t,x)$$
$$\phi_2^T(t,x)\ \psi^T(t_k,x)\ \psi^T(t_{k+1},x)\ \tilde{\psi}^T(t_k,x)\,\varphi^T(\mathcal{K}_j\tilde{\psi}(t_k,x))\Big]^T,$$
$$d_1(t)=t-t_k,\ d_2(t)=t_{k+1}-t,\ \mathscr{E}_r=\Big[0_{n\times(r-1)n}\ I_n\ 0_{n\times(13-r)n}\Big],$$
$$\bar{\phi}(s,x)=\Big[\psi^T(s,x)\ \ g(t,x)\Big]^T,\ \phi_0^T(x)=\frac{1}{d_k}\int_{t_k}^{t_{k+1}}\psi^T(s,x)ds,\ \phi_1^T(t,x)=\frac{1}{d_1(t)}\int_{t_k}^{t}\psi^T(s,x)ds,$$
$$\phi_2^T(t,x)=\frac{1}{d_2(t)}\int_{t}^{t_{k+1}}\psi^T(s,x)ds,\ \phi_3(t,x)=[\psi^T(t,x)\ \ \psi^T(t_k,x)\ \ \psi^T(t_{k+1},x)]^T,$$
$$\phi_4(t,x)=[\psi^T(t_k,x)\ \ \psi^T(t_{k+1},x)]^T,\ \phi_5(t,x)=\psi(t,x)-\psi(t_k,x),\ \phi_6(t,x)=\psi(t_{k+1},x)-\psi(t,x).$$

B. Appendix-B

$$\Phi_1=[\mathcal{E}_1^T\quad\mathcal{E}_5^T]^T\ ,\ \Phi_2=[\mathcal{E}_3^T\quad\mathcal{E}_6^T]^T,\ \Phi_3=[\mathcal{E}_{10}^T\quad\mathcal{E}_{11}^T]^T,\ \Phi_4=\mathcal{E}_1-\mathcal{E}_{10},\ \Phi_5=\mathcal{E}_{11}-\mathcal{E}_1,$$
$$\Phi_6=\mathcal{E}_{11}-\mathcal{E}_{10},\Phi_7=[\mathcal{E}_1^T\quad\mathcal{E}_{10}^T\quad\mathcal{E}_8^T]^T,\Phi_8=\mathcal{E}_1+\mathcal{E}_{10}-2\mathcal{E}_8,\ \Phi_9=[\mathcal{E}_{11}^T\quad\mathcal{E}_1^T\quad\mathcal{E}_9^T]^T,$$
$$\Phi_{10}=\mathcal{E}_{11}+\mathcal{E}_1-2\mathcal{E}_9,\ P(t)=[\sigma(t)P_{1i}+(\bar{\sigma}-\sigma(t))P_{2i}],\ \Xi_1(t)=\mathcal{E}_1^T\sum_{i=1}^{\iota}\lambda_i[P(t)+G_1]\mathcal{E}_1,$$
$$\Xi_2=\Phi_1^T\sum_{i=1}^{\iota}\lambda_i[(R_{1i}+G_2)-(1-\mathfrak{d})T_1]\Phi_1,\ \Xi_3=\mathcal{E}_1^T\sum_{i=1}^{\iota}\lambda_i[(R_{2i}+G_3)-T_2]\mathcal{E}_1,$$
$$\mathfrak{Q}_1=\int_\Gamma\psi^T(t,x)\sum_{i=1}^{\iota}\dot{\mathfrak{h}}_i(\mathscr{C}(t))P(t)\psi(t,x)dx,\ \mathfrak{Q}_2=\int_\Gamma\int_{t-\sigma(t)}^{t}\bar{\phi}^T(s,x)(\sum_{i=1}^{\iota}\dot{\mathfrak{h}}_i(\mathscr{C}(t))R_{1i})\bar{\phi}(s,x)dsdx,$$
$$\mathfrak{Q}_3=\int_\Gamma\int_{t-\bar{\sigma}}^{t}\psi^T(s,x)(\sum_{i=1}^{\iota}\dot{\mathfrak{h}}_i(\mathscr{C}(t))R_{2i})\psi(s,x)dsdx,\ \mathfrak{Q}_4=-\int_\Gamma\int_{t-\sigma(t)}^{t}\bar{\phi}^T(t,x)T_1\bar{\phi}(t,x)dsdx,$$
$$\mathfrak{Q}_5=-\int_\Gamma\int_{t-\bar{\sigma}}^{t}\psi^T(s,x)T_2\psi(s,x)dsdx,\ \mathfrak{A}[t,\sigma(t)]=\mathfrak{C}[t,\sigma(t)]-\mathfrak{F},$$
$$\Sigma[t,\sigma(t)]=\sum_{i=1}^{\iota}\mathfrak{h}_i(\mathscr{C}(t))\Big\{\mathcal{E}_1^TP(t)\mathcal{E}_2+\mathfrak{d}\mathcal{E}_1^T(P_{1i}-P_{2i})\mathcal{E}_1+\Phi_1^TR_{1i}\Phi_1+\mathcal{E}_1^TR_{2i}\mathcal{E}_1-\mathcal{E}_4^TR_{2i}\mathcal{E}_4^T$$

$$
\begin{aligned}
&- (1-\eth)\Phi_2^T R_{1i}\Phi_2\Big\} + \sigma(t)\Phi_1^T T_1\Phi_1 + \bar{\sigma}\mathcal{E}_1^T T_2\mathcal{E}_1 - \mathcal{E}_{12}^T S\mathcal{E}_{12} + \mathbf{sym}\{\mathcal{E}_1^T Y_2\Phi_3 + \mathcal{E}_1^T Y_4\mathcal{E}_8\\
&+ \mathcal{E}_2^T W_1\Phi_4\} + d_1(t)\mathbf{sym}\{\mathcal{E}_2^T Y_2\Phi_3 + \mathcal{E}_2^T Y_1\mathcal{E}_1 + \mathcal{E}_1^T Y_3\mathcal{E}_8\} + \mathcal{E}_1^T Y_1\mathcal{E}_1 - \mathcal{E}_8^T Y_4\mathcal{E}_8\\
&+ \mathbf{sym}\{\mathcal{E}_1^T H_2\Phi_3 + \mathcal{E}_1^T H_3\mathcal{E}_1 - \mathcal{E}_2^T W_2\Phi_5\} - d_2(t)\mathbf{sym}\{\mathcal{E}_2^T H_1\mathcal{E}_1 + \mathcal{E}_2^T H_2\Phi_3\\
&+ \mathcal{E}_2^T H_3\mathcal{E}_9\} + \mathcal{E}_1^T H_1\mathcal{E}_1 + \mathcal{E}_2^T(d_2(t)U_1 + d_1(t)U_2)\mathcal{E}_2,\\
\mathfrak{C}[t,\sigma(t)] &= \Sigma[t,\sigma(t)] + \Xi_1(t) + \mathbf{sym}\{-\mathcal{E}_1^T NA_\pi\mathcal{E}_1 - [\mathcal{E}_5 - \Gamma_1\mathcal{E}_1]^T\Lambda_1[\mathcal{E}_5 - \Gamma_2\mathcal{E}_1]\\
&- [\mathcal{E}_6 - \Gamma_1\mathcal{E}_3]^T\Lambda_2[\mathcal{E}_6 - \Gamma_2\mathcal{E}_3] + \bar{\varphi}\mathcal{E}_{12}^T\mathcal{K}_j^T\Lambda_3\mathcal{K}_j\mathcal{E}_{12} - \mathcal{E}_{13}^T\Lambda_3\mathcal{E}_{13} + (o_1\mathcal{E}_1^T + o_2\mathcal{E}_2^T)N(-B_i\mathcal{E}_1\\
&+ C_i\mathcal{E}_5 + D_i\mathcal{E}_6 + \mathcal{K}_j\mathcal{E}_{12} - \mathcal{E}_{13} - \mathcal{E}_2)\} + \mathbf{sym}\Big\{\Phi_7^T M_1\Phi_4 + \Phi_7^T M_2\Phi_8 + \Phi_9^T M_3\Phi_5 + \Phi_9^T M_4\Phi_{10}\Big\},\\
\mathfrak{F} &= \mathbf{sym}\{\mathcal{E}_{11}^T Y_2\Phi_3 + \mathcal{E}_{10}^T H_2\Phi_3 + \mathcal{E}_{10}^T H_3\mathcal{E}_7\} + \mathcal{E}_{11}^T Y_1\mathcal{E}_{11}\\
&+ \mathcal{E}_{10}^T H_1\mathcal{E}_{10} + d_k\mathcal{E}_7^T Y_3\mathcal{E}_7 + \mathcal{E}_7^T Y_4\mathcal{E}_7 + \Phi_6^T(U_1 - U_2)\Phi_6.
\end{aligned}
$$

C. Appendix-C

$$
\begin{aligned}
V_1(t) &= \int_\Gamma \psi^T(t,x)\sum_{i=1}^{\iota}\mathfrak{h}_i(\mathscr{C}(t))P(t)\psi(t,x)dx,\\
V_2(t) &= \int_\Gamma\int_{t-\sigma(t)}^{t}\bar{\phi}^T(s,x)\sum_{i=1}^{\iota}\mathfrak{h}_i(\mathscr{C}(t))R_{1i}\bar{\phi}(s,x)dsdx + \int_\Gamma\int_{t-\bar{\sigma}}^{t}\psi^T(s,x)\sum_{i=1}^{\iota}\mathfrak{h}_i(\mathscr{C}(t))R_{2i}\psi(s,x)dsdx,\\
V_3(t) &= \int_\Gamma\int_{t-\sigma(t)}^{t}\int_u^t\bar{\phi}^T(s,x)T_1\bar{\phi}(s,x)dsdudx + \int_\Gamma\int_{t-\bar{\sigma}}^{t}\int_u^t\psi^T(s,x)T_2\psi(s,x)dsdudx,\\
V_4(t) &= \int_\Gamma(t_{k+1}-t)\tilde{\psi}^T(t_k,x)S\tilde{\psi}(t_k,x)dx,\ V_5(t) = 2\int_\Gamma\sum_{l=1}^{m}\frac{\partial\psi^T(t,x)}{\partial x_l}NA_l\frac{\partial\psi(t,x)}{\partial x_l}dx,\\
V_6(t) &= \int_\Gamma d_1(t)\psi^T(t,x)[Y_1\ 2Y_2]\phi_3(t,x)dx + \int_\Gamma d_1(t)\phi_1^T(t,x)Y_3d_1(t)\phi_1(t,x)dx\\
&+ \int_\Gamma d_1(t)\phi_1^T(t,x)Y_4\phi_1(t,x)dx + \int_\Gamma d_k\phi_5^T(t,x)W_1\phi_5(t,x)dx,\\
V_7(t) &= -\int_\Gamma d_2(t)\psi^T(t,x)[H_1\ 2H_2]\phi_3(t,x)dx - \int_\Gamma 2\psi^T(t,x)H_3d_2(t)\phi_2(t,x)dx\\
&+ \int_\Gamma d_k\phi_6^T(t,x)W_2\phi_6(t,x)dx,\\
V_8(t) &= d_2(t)\int_\Gamma\int_{t_k}^{t}\frac{\partial\psi^T(s,x)}{\partial s}U_1\frac{\partial\psi(s,x)}{\partial s}dsdx - d_1(t)\int_\Gamma\int_t^{t_{k+1}}\frac{\partial\psi^T(s,x)}{\partial s}U_2\frac{\partial\psi(s,x)}{\partial s}dsdx.
\end{aligned}
$$